Dynamical model of J/ψ photoproduction on the nucleon

S. Sakinah [1,*] T.-S. H. Lee [2,†] and H. M. Choi [1,‡]
[1]*Department of Physics, Kyungpook National University, Daegu 41566, South Korea*
[2]*Physics Division, Argonne National Laboratory, Argonne, Illinois 60439, USA*

(Received 5 March 2024; revised 10 April 2024; accepted 21 May 2024; published 13 June 2024)

A dynamical model based on a phenomenological charm quark-nucleon (c-N) potential v_{cN} and the Pomeron-exchange mechanism is constructed to investigate the J/ψ photoproduction on the nucleon from threshold to invariant mass $W = 300$ GeV. The J/ψ-N potential, $V_{J/\psi N}(r)$, is constructed by folding v_{cN} into the wave function $\phi_{J/\psi}(c\bar{c})$ of J/ψ within a constituent quark model (CQM) of Segovia *et al.* [Int. J. Mod. Phys. E **22**, 1330026 (2013)]. A photoproduction amplitude is also generated by v_{cN} by a $c\bar{c}$-loop integration over the $\gamma \to c\bar{c}$ vertex function and $\phi_{J/\psi}(c\bar{c})$. No commonly used vector meson dominance assumption is used to define this photoproduction amplitude which is needed to describe the data near the threshold. The c-N potential $v_{cN}(r)$ is parameterized in a form such that the predicted $V_{J/\psi N}(r)$ at large distances has the same Yukawa potential form extracted from a lattice QCD (LQCD) calculation of Kawanai and Sasaki, [Phys. Rev. D **82**, 091501(R) (2010)]. The parameters of v_{cN} are determined by fitting the total cross-section data of Jefferson Laboratory (JLab) by performing calculations that include J/ψ-N final-state interactions (FSI). The resulting differential cross sections $d\sigma/dt$ are found in good agreements with the data. It is shown that the FSI effects dominate the cross section in the very near-threshold region, allowing for sensitive testing of the predicted J/ψ-N scattering amplitudes. By imposing the constraints of J/ψ-N potential extracted from the LQCD calculation of Kawanai and Sasaki, [Phys. Rev. D **82**, 091501(R) (2010)], we have obtained three J/ψ-N potentials which fit the JLab data equally well. The resulting J/ψ-N scattering lengths are in the range of $a = [-0.05, -0.25]$ fm. With the determined $v_{cN}(r)$ and the wave functions generated from the same CQM, the constructed model is used to predict the cross sections of photoproduction of $\eta_c(1S)$ and $\psi(2S)$ mesons for future experimental tests.

DOI: 10.1103/PhysRevC.109.065204

I. INTRODUCTION

It is well recognized [1] that the information on the interactions between the J/ψ meson and the nucleon (N) can improve our understanding of the roles of gluons (g) in determining the structure of hadrons and hadron-hadron interactions. In addition, a model of the J/ψ-N interaction is needed to understand the nucleon resonances $N^*(P_c)$ reported by the LHCb collaboration [2–5]. It is also needed to extract the gluonic distributions in nuclei and to study the existence of nuclei with hidden charms [6–10].

The leading J/ψ-N interaction is the two-gluon exchange mechanism, as illustrated in Fig. 1. Higher-order multigluon exchange effects cannot be neglected in the nonperturbative region. By using continuum and lattice studies at low energies and the heavy quark effective field theory and perturbative QCD at high energies, the J/ψ-N interaction can be estimated.

Several attempts had been made to determine the J/ψ-N interactions. Peskin [11] applied the operator product expansion to evaluate the strength of the color field emitted by heavy $q\bar{q}$ systems and suggested [12] that the van der Waals force induced by the color field of J/ψ on nucleons can generate an attractive short-range J/ψ-N interaction. The results of Peskin were used by Luke, Manohar, and Savage [13] to predict, using the effective field theory method, the J/ψ-N forward scattering amplitude which was then used to get an estimation that J/ψ can have a few MeV-per-nucleon attraction in nuclear matter. The J/ψ-N forward scattering amplitude of Ref. [13] was further investigated by Brodsky and Miller [14] to derive a J/ψ-N potential which gives a J/ψ-N scattering length of -0.24 fm. The result of Peskin was also used by Kaidalov and Volkovitsky [15], who differed from Ref. [14] in evaluating the gluon content in the nucleon, to give a much smaller scattering length of -0.05 fm. In a lattice QCD (LQCD) calculation using the approach of Refs. [16,17], Kawanai and Sasaki [18–20] obtained an attractive J/ψ-N potential of the Yukawa form $V_{J/\psi N, J/\psi N} = -\alpha e^{-\mu r}/r$ with $\alpha = 0.1$ and $\mu = 0.6$ GeV, which gives a scattering length of -0.09 fm.

To make progress, it is necessary to have experimental information on the J/ψ-N scattering to test the theoretical results described above and future LQCD calculations. One can employ the traditional approach to determine the vector meson-nucleon (VN) interaction by applying the vector meson dominance (VMD) assumption. This method is commonly used to extract J/ψ-N cross sections from the

*Contact author: ssakinahf@knu.ac.kr
†Contact author: tshlee@anl.gov
‡Contact author: homyoung@knu.ac.kr

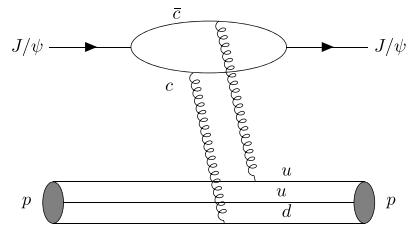

FIG. 1. Two gluon exchange mechanism of $\gamma + N \to J/\psi + N$ reaction.

data of J/ψ photoproduction reactions. In this approach, the incoming photon is converted into a vector meson V which is then scattered from the nucleon, as illustrated in Fig. 2. However, the approach based on VMD is not valid for J/ψ because the VMD coupling constant is determined by the $J/\psi \to \gamma \to e^+e^-$ decay width at $q^2 = m^2_{J/\psi} \approx 9$ GeV^2 which is far from $q^2 = 0$ of the $\gamma + p \to J/\psi + p$ reaction. Furthermore, the use of VMD for J/ψ is questionable as discussed in Refs. [21,22]. In addition, the transition amplitude $t_{J/\psi N,J/\psi N}(k, q, W)$ for $J/\psi + N \to J/\psi + N$ near threshold is far off-shell. For instance, at $W = (m_N + m_{J/\psi}) + 0.5$ GeV, the incoming γN relative momentum is $q = 0.8$ GeV, which is much larger than the outgoing J/ψ-N relative momentum $k = 0.1$ GeV in the center-of-mass system. Thus, the VMD approach is clearly not directly applicable for describing $J/\psi + N \to J/\psi + N$ in the near-threshold energy region.

In this paper, we present a reaction model to extract the J/ψ-N scattering amplitudes from the data of $\gamma + N \to J/\psi + N$ reactions, specifically from the experiments at Jefferson Laboratory (JLab) [23–25]. In the meantime, we will obtain phenomenological J/ψ-N potentials, $V_{J/\psi N,J/\psi N}$, for investigating nuclear reactions involving J/ψ meson. No VMD is assumed by taking the $c\bar{c}$ structure of J/ψ into account to define the model Hamiltonian. For simplicity in this exploring work, we will follow the Pomeron-exchange model of Donnachie and Landshoff (DL) [26] to neglect the quark substructure of the nucleon and assume that the interactions between the charm-anticharm ($c\bar{c}$) quarks in J/ψ and the nucleon can be defined by a phenomenological quark-N potential v_{cN}. It follows that the $\gamma + N \to J/\psi + N$ transition amplitude, $B_{\gamma N,J/\psi N}$, and the $J/\psi + N \to J/\psi + N$ potential, $V_{J/\psi N}$, are defined by $c\bar{c}$-loop mechanisms, as illustrated in Fig. 3. Following the dynamical formulation [27–30] within

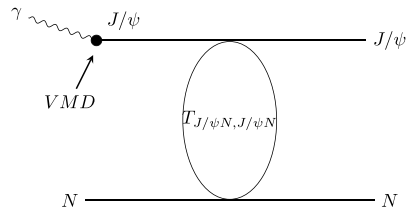

FIG. 2. The $\gamma + N \to J/\psi + N$ reaction within the model based on the VMD assumption.

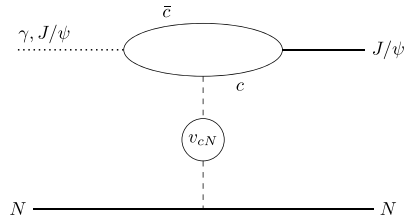

FIG. 3. Quark-antiquark loop mechanism of $\gamma + N \to J/\psi + N$ and $J/\psi + N \to J/\psi + N$ due to a phenomenological charm quark-nucleon (c-N) potential v_{cN}.

which the unitarity condition requires that J/ψ-N final-state interaction (FSI) effects must be included, the total amplitude of $\gamma + N \to J/\psi + N$ then has the following form:

$$T^D_{\gamma N,J/\psi N} = B_{\gamma N,J/\psi N} + T^{(\mathrm{fsi})}_{\gamma N,J/\psi N}, \tag{1}$$

with

$$T^{(\mathrm{fsi})}_{\gamma N,J/\psi N} = B_{\gamma N,J/\psi N}\; G_{J/\psi N}\; T_{J/\psi N,J/\psi N}, \tag{2}$$

where $G_{J/\psi N}$ is the J/ψ-N propagator and $T_{J/\psi N,J/\psi N}$ is the J/ψ-N scattering amplitude calculated from the J/ψ-N potential, $V_{J/\psi N}$, by solving the following Lippman-Schwinger equation:

$$T_{J/\psi N,J/\psi N} = V_{J/\psi N,J/\psi N} + V_{J/\psi N,J/\psi N}\, G_{J/\psi N}\, T_{J/\psi N,J/\psi N}. \tag{3}$$

To also describe data up to 300 GeV [23–25,31,32], we add the Pomeron-exchange amplitude $T^{\mathrm{Pom}}_{\gamma N,J/\psi N}$ of DL [26], reviewed in Ref. [1], such that the total amplitude can be used to investigate nuclear reactions involving J/ψ at all energies. To be consistent, the Pomeron-exchange amplitude should also be defined by the similar $c\bar{c}$-loop mechanism of Fig. 3. By using a hadron model [33,34] based on Dyson-Schwinger equation (DSE) of QCD, such a quark-loop Pomeron-exchange model was explored in Refs. [35,36]. It will be interesting to use the recent DSE models [37–44] to improve the results of Refs. [35,36]. Within the Hamiltonian formulation of this work, it requires a realistic constituent quark model (CQM) to generate the J/ψ wave function and careful treatments of relativistic kinematic effects within Dirac's formulation of relativistic quantum mechanics [45]. We therefore will not pursue this here. Rather we focus on the near-threshold region, and any effects from Pomeron-exchange which is very weak in the near threshold region, can be considered as an estimate of the uncertainties of the results presented in this paper.

Since the Pomeron-exchange amplitude $T^{\mathrm{Pom}}_{\gamma N,J/\psi N}$ has been determined in Ref. [1], our task is to develop a model for calculating the amplitude $T^D_{\gamma N,J/\psi N}$ defined by Eqs. (1)–(3). As defined by the loop-mechanism illustrated in Fig. 3, the J/ψ-N potential $V_{J/\psi N}(r)$ is constructed by folding $v_{cN}(r)$ into the J/ψ wave function $\phi_{J/\psi}$. By using $\phi_{J/\psi}$ from the CQM of Ref. [46], the amplitude $T^D_{\gamma N,J/\psi N}$ is completely determined by $v_{cN}(r)$. To establish correspondence with the LQCD calculations, the parametrization of $v_{cN}(r)$ is chosen such that

the predicted $V_{J/\psi N}(r)$ at large distances exhibits the same Yukawa potential form extracted from a LQCD calculation of Refs. [18,20].

We determine the parameters of v_{cN} by fitting the total cross-section data from the JLab experiments [23,24]. As will be presented later, the resulting differential cross sections $d\sigma/dt$ are in reasonably good agreements with the data [23–25] from JLab. More importantly, it is shown that the FSI effects dominate the cross section in the very near-threshold region, allowing for sensitive testing of the predicted J/ψ-N scattering amplitudes. Within the experimental uncertainties, this procedure allows us to obtain several J/ψ-N potentials which all fit the available JLab data reasonably well. They, however, predict rather different cross sections near threshold and the resulting J/ψ-N scattering lengths. More extensive and precise data in the very near threshold region are needed for making further progress.

By using the determined c-N potential $v_{cN}(r)$ and the wave functions generated from the same CQM of Ref. [46], we can apply the constructed dynamical model to predict the cross sections of photoproduction of the other charmonium states. The results for the production of $\eta_c(1S)$ and $\psi(2S)$ mesons are presented for future experimental tests at JLab and the future electron-ion colliders (EIC).

Here we note that the JLab data of J/ψ photoproduction had also been investigated by using models based on two- and three-gluons exchange mechanisms [47], generalized parton distribution of the nucleon [48], and the holographic QCD [49]. All of these approaches have rather different assumptions in treating the quark substructure of J/ψ. They are distinctively different from our approach which accounts for the $c\bar{c}$-loop mechanisms in calculating both the J/ψ photoproduction amplitudes and J/ψ-N final-state interactions. Thus their objective is not to extract J/ψ-N interactions at low energies, as we are trying to achieve in this work.

Without using VMD, the JLab data had also been investigated [21] by using the effective Lagrangian approach. Their objective was to demonstrate that with appropriate parameters the cusp structure of JLab data at $W \approx 4.2$–4.3 GeV can be explained by the box-diagram mechanisms $\gamma N \to \bar{D}^* \Lambda_c \to J/\psi N$ due to the exchanges of $\bar{D}^*$ and Λ_c mesons. This approach can in principle be extended to extract J/ψ-N interaction from J/ψ photoproduction data but has not been pursued.

In Sec. II, we present our formulation. The results are presented in Sec. III. In Sec. IV, we provide a summary and discuss possible future improvements.

II. FORMULATION

We follow Ref. [50] to use the normalization $\langle \mathbf{k}|\mathbf{k}'\rangle = \delta(\mathbf{k}-\mathbf{k}')$ for plane-wave state $|\mathbf{k}\rangle$ and $\langle \phi_\alpha|\phi_\beta\rangle = \delta_{\alpha,\beta}$ for bound state $|\phi_\alpha\rangle$. The J/ψ meson will be denoted as V in the rest of the paper.

In the center-of-mass frame, the differential cross section of vector meson (V) photoproduction reaction, $\gamma(\mathbf{q},\lambda_\gamma) + N(-\mathbf{q}, m_s) \to V(\mathbf{k},\lambda_V) + N(-\mathbf{k}, m_s')$, is calculated from [1]

$$\frac{d\sigma_{VN,\gamma N}}{d\Omega} = \frac{(2\pi)^4}{|\mathbf{q}|^2}\frac{|\mathbf{k}|\,E_V(\mathbf{k})E_N(\mathbf{k})}{W}\frac{|\mathbf{q}|^2 E_N(\mathbf{q})}{W} \times \frac{1}{4}\sum_{\lambda_V, m_s'}\sum_{\lambda_\gamma, m_s} |\,\langle \mathbf{k},\lambda_V m_s'|T_{VN,\gamma N}(W)|\mathbf{q},\lambda_\gamma m_s\rangle\,|^2, \tag{4}$$

where m_s (m_s') denotes the z component of the initial- (final-) state nucleon spin, and λ_V and λ_γ are the helicities of vector meson V and photon γ, respectively. The magnitudes $q = |\mathbf{q}|$ and $k = |\mathbf{k}|$ are defined by the invariant mass $W = q + E_N(q) = E_V(k) + E_N(k)$.

The reaction amplitude $T_{VN,\gamma N}(W)$ can be decomposed into the sum of the dynamical scattering amplitude $T^D_{VN,\gamma N}(W)$ and the Pomeron-exchange amplitude $T^{\rm Pom}_{VN,\gamma N}(W)$ as [1]

$$T_{VN,\gamma N}(W) = T^D_{VN,\gamma N}(W) + T^{\rm Pom}_{VN,\gamma N}(W). \tag{5}$$

We shall describe each amplitude in the following subsections.

A. Dynamical model for $T^D_{VN,\gamma N}(W)$

Following the dynamical approach of Refs. [27–30], the amplitude $T^D_{VN,\gamma N}(W)$ is calculated from using the following Hamiltonian:

$$H = H_0 + \Gamma_{\gamma,c\bar{c}} + v_{c\bar{c}} + v_{cN}, \tag{6}$$

where H_0 is the free Hamiltonian, v_{cN} is a phenomenological quark-nucleon potential to be determined, $v_{c\bar{c}}$ is the $c\bar{c}$ potential of CQM, and $\Gamma_{\gamma,c\bar{c}}$ is the electromagnetic coupling of $\gamma \to c\bar{c}$ defined by

$$\langle \mathbf{q}|\Gamma_{\gamma,c\bar{c}}|\mathbf{k}_1,\mathbf{k}_2\rangle = \frac{1}{\sqrt{2|\mathbf{q}|}}\frac{1}{\sqrt{2E_c(\mathbf{k}_1)}}\frac{1}{\sqrt{2E_c(\mathbf{k}_2)}} \times \frac{e_c}{(2\pi)^{3/2}}[\bar{u}(\mathbf{k}_1)\gamma^\mu \epsilon_\mu(q) v(\mathbf{k}_2)]. \tag{7}$$

Here e_c is the charge of the charmed quark, $\epsilon_\mu(q)$ is the photon polarization vector, and $\bar{u}(\mathbf{k}_1)$ and $v(\mathbf{k}_2)$ are the Dirac spinors with the normalization $\bar{u}(\mathbf{k})u(\mathbf{k}) = \bar{v}(\mathbf{k})v(\mathbf{k}) = 1$.

Using the potential $v_{c\bar{c}}$ in the Hamiltonian, the wave function $|\phi_V\rangle$ of the J/ψ is obtained by solving the bound-state equation within a CQM developed by Segovia *et al.* [46], expressed as:

$$(H_0 + v_{c\bar{c}})\,|\phi_V\rangle = E_V\,|\phi_V\rangle\,. \tag{8}$$

Here we assume a simple s-wave wave function defined in momentum space as

$$\phi^{J_V m_V}_{V,\mathbf{p}_V}(\mathbf{k} m_{s_c}, \mathbf{k}' m'_{s_c}) = \left\langle J_V m_V \middle| \tfrac{1}{2}\tfrac{1}{2} m_{s_c} m'_{s_{\bar{c}}}\right\rangle \phi(\bar{\mathbf{k}})\delta(\mathbf{p}_V - \mathbf{k} - \mathbf{k}'), \tag{9}$$

where $\mathbf{p}_V$ is the momentum of J/ψ, $\mathbf{k}(\mathbf{k}')$ is the momentum of $c(\bar{c})$, and $\bar{\mathbf{k}} = (\mathbf{k}-\mathbf{k}')/2$. The total angular momentum and its magnetic quantum number of J/ψ are denoted by J_V and m_V, respectively, and $m_{s_c}(m'_{s_{\bar{c}}})$ is the magnetic quantum number of $c(\bar{c})$ spin angular momentum.

With the Hamiltonian given by Eq. (6) and neglecting the quark-quark scattering, the scattering amplitude $T(W)$

for $\gamma + N \to V + N$ process is defined by the following Lippmann-Schwinger equation:

$$T(W) = H' + T(W)\frac{1}{W - H_0 + i\epsilon}H', \tag{10}$$

where

$$H' = \Gamma_{\gamma,c\bar{c}} + v_{cN}. \tag{11}$$

Inserting the intermediate states of $|VN\rangle$, $|c\bar{c}N\rangle$ and keeping only the first order in electromagnetic coupling e in Eq. (10), we obtain

$$T^D_{VN,\gamma N}(W) = B_{VN,\gamma N}(W) + T^{(\mathrm{fsi})}_{VN,\gamma N}(W), \tag{12}$$

where $B_{VN,\gamma N}(W)$ is the Born term of J/ψ photoproduction and the FSI term $T^{(\mathrm{fsi})}_{VN,\gamma N}(W)$ is required by the unitary condition and is defined by

$$T^{(\mathrm{fsi})}_{VN,\gamma N}(W) = T_{VN,VN}(W)\frac{1}{W - H_0 + i\epsilon}B_{VN,\gamma N}(W). \tag{13}$$

In this work, we assume that the VN potential can be constructed by the Folding model [51] using the quark-N interaction v_{cN} and the wave function ϕ_V generated from Eq. (8),

$$V_{VN,VN} = \langle \phi_V, N| \sum_c v_{cN} |\phi_V, N\rangle . \tag{14}$$

The wave function and v_{cN} potential are also used to construct the J/ψ photoproduction process with the following form:

$$B_{VN,\gamma N}(W) = \langle \phi_V, N| \left[\sum_c v_{cN} \frac{|c\bar{c}\rangle \langle c\bar{c}|}{E_{c\bar{c}} - H_0} \Gamma_{\gamma,c\bar{c}} \right] |\gamma, N\rangle , \tag{15}$$

where $E_{c\bar{c}}$ is the energy available to the propagation of $c\bar{c}$.

In the following, we give explicit expressions of the matrix elements of $V_{VN,VN}$, $B_{VN,\gamma N}(W)$, and $T^{(\mathrm{fsi})}_{VN,\gamma N}(W)$.

1. Matrix elements of $V_{VN,VN}$

To evaluate Eq. (14), we assume for simplicity that quark-N interaction, v_{cN}, is independent of spin variables,

$$\langle \mathbf{k}\, m_{s_c}, \mathbf{p}\, m_{s_N} |\, v_{cN}\, |\mathbf{k}'\, m'_{s_c}, \mathbf{p}'\, m'_{s_N}\rangle = \delta_{m_{s_c},m'_{s_c}} \delta_{m_{s_N},m'_{s_N}} \delta(\mathbf{k} + \mathbf{p} - \mathbf{k}' - \mathbf{p}') \langle \mathbf{q}|v_{cN}|\mathbf{q}'\rangle , \tag{16}$$

where the relative momenta of quark and nucleon are defined by

$$\mathbf{q} = \frac{m_N\mathbf{k} - m_c\mathbf{p}}{m_N + m_c}, \tag{17}$$

$$\mathbf{q}' = \frac{m_N\mathbf{k}' - m_c\mathbf{p}'}{m_N + m_c}. \tag{18}$$

Here m_c and m_N are the masses of the quark c and the nucleon, respectively.

With the J/ψ wave function given in Eq. (9) and the spin-independent quark-N potential defined by Eq. (16), we can evaluate the matrix element of the potential $V_{VN,VN}$ given by Eq. (14). In the center-of-mass frame, where $\mathbf{p}_V = -\mathbf{p}$ and $\mathbf{p}'_V = -\mathbf{p}'$ as illustrated in Fig. 4, we then have

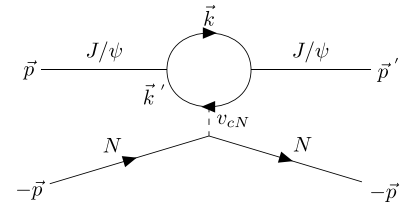

FIG. 4. J/ψ-N potential defined by the quark-nucleon potential v_{cN}, with the momentum variables in Eq. (20).

$$\langle \mathbf{p}_V m_V, \mathbf{p} m_s | V_{VN,VN} | \mathbf{p}'_V m'_V, \mathbf{p}' m'_s\rangle = \delta_{m_V,m'_V}\delta_{m_s,m'_s}\delta(\mathbf{p}_V + \mathbf{p} - \mathbf{p}'_V - \mathbf{p}') \langle \mathbf{p}|V_{VN}|\mathbf{p}'\rangle , \tag{19}$$

where

$$\langle \mathbf{p}|V_{VN}|\mathbf{p}'\rangle = 2\int d\mathbf{k}\, \phi^*\left(\mathbf{k} - \tfrac{\mathbf{p}}{2}\right) \times \left\langle \mathbf{p} - \frac{m_N}{m_N + m_c}\mathbf{k}\right| v_{cN} \left| \mathbf{p}' - \frac{m_N}{m_N + m_c}\mathbf{k}\right\rangle \times \phi\left(\mathbf{k} - \tfrac{\mathbf{p}'}{2}\right). \tag{20}$$

Here the factor 2 arises from the summation of the contributions from the two quarks within the J/ψ meson and we have used the definitions of Eqs. (17) and (18).

For a potential $v_{cN}(r)$ depending only on the relative distance r between c and N, we have

$$\langle \mathbf{q}|v_{cN}|\mathbf{q}'\rangle = v_{cN}(\mathbf{q} - \mathbf{q}') = \frac{1}{(2\pi)^3}\int d\mathbf{r}\, e^{i(\mathbf{q}-\mathbf{q}')\cdot\mathbf{r}} v_{cN}(r). \tag{21}$$

The matrix element of v_{cN} in Eq. (20) can then be written as

$$\left\langle \mathbf{p} - \frac{m_N}{m_N + m_c}\mathbf{k}\right| v_{cN} \left| \mathbf{p}' - \frac{m_N}{m_N + m_c}\mathbf{k}\right\rangle = v_{cN}(\mathbf{p} - \mathbf{p}'). \tag{22}$$

For later calculations, we note here that for a Yukawa form $v_{cN}(r) = \alpha\frac{e^{-\mu r}}{r}$, Eq. (21) leads to

$$v_{cN}(\mathbf{p} - \mathbf{p}') = \alpha\frac{1}{(2\pi)^2}\frac{1}{(\mathbf{p} - \mathbf{p}')^2 + \mu^2}. \tag{23}$$

Using Eq. (22), Eq. (20) can now be expressed in the following factorized form:

$$\langle \mathbf{p}|V_{VN}|\mathbf{p}'\rangle = F_V(\mathbf{t})[2v_{cN}(\mathbf{t})], \tag{24}$$

where $\mathbf{t} = \mathbf{p} - \mathbf{p}'$, and

$$F_V(\mathbf{t}) = \int d\mathbf{k}\, \phi^*\left(\mathbf{k} - \frac{\mathbf{p}}{2}\right)\phi\left(\mathbf{k} - \frac{\mathbf{p}'}{2}\right) = \int d\mathbf{k}\, \phi^*\left(\mathbf{k} - \frac{\mathbf{t}}{2}\right)\phi(\mathbf{k}) \tag{25}$$

is the form factor of the vector meson V and $\phi(\mathbf{k})$ is the wave function of J/ψ in momentum space.

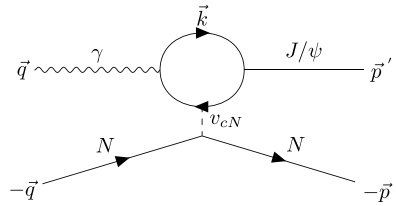

FIG. 5. J/ψ photoproduction on the nucleon target with the momentum variables indicated in Eq. (29).

2. Matrix element of $B_{VN,\gamma N}(W)$

By using the J/ψ wave function and Eq. (16) for quark-N potential, the matrix element of photoproduction of Eq. (15) can be calculated. With the variables in the center-of-mass system, as illustrated in Fig. 5, we obtain

$$\begin{aligned}
&\langle \mathbf{p}' m_V m_s' \,|\, B_{VN,\gamma N}(W) \,|\, \mathbf{q}\lambda m_s\rangle \\
&= \sum_{m_c,m_{\bar c}} \frac{1}{(2\pi)^3}\frac{e_c}{\sqrt{2|\mathbf{q}|}} \int d\mathbf{k} \left\langle J_V m_V \middle| \frac{1}{2}\frac{1}{2} m_c m_{\bar c}\right\rangle \phi\left(\mathbf{k}-\frac{1}{2}\mathbf{p}'\right) \\
&\times \delta_{m_s,m_s'} \left\langle \mathbf{p}' - \frac{m_N}{m_N+m_c}\mathbf{k} \middle| v_{cN} \middle| \mathbf{q} - \frac{m_N}{m_N+m_c}\mathbf{k}\right\rangle \\
&\times \frac{1}{W - E_N(\mathbf{q}) - E_c(\mathbf{q}-\mathbf{k}) - E_c(\mathbf{k}) + i\epsilon} \\
&\times \bar u_{m_c}(\mathbf{k})[\epsilon_\lambda \cdot \gamma] v_{m_{\bar c}}(\mathbf{q}-\mathbf{k}).
\end{aligned} \tag{26}$$

If one chooses the Yukawa form for $v_{cN}(r)$, then one obtains the following factorized form:

$$\begin{aligned}
&\langle \mathbf{p}' m_V m_s' \,|\, B_{VN,\gamma N}(W) \,|\, \mathbf{q}\lambda m_s\rangle \\
&\quad = C_{\lambda,m_V}\delta_{m_s,m_s'} B(\mathbf{p}', \mathbf{q}, W)[2v_{cN}(\mathbf{q}-\mathbf{p}')],
\end{aligned} \tag{27}$$

where

$$C_{\lambda,m_V} = \sum_{m_c,m_{\bar c}} \left\langle J_V m_V \middle| \frac{1}{2}\frac{1}{2} m_c m_{\bar c}\right\rangle \langle m_{\bar c}|\sigma\cdot\epsilon_\lambda|m_c\rangle\,, \tag{28}$$

and

$$\begin{aligned}
B(\mathbf{p}', \mathbf{q}, W) = &\frac{1}{(2\pi)^3}\frac{e_c}{\sqrt{2|\mathbf{q}|}} \int d\mathbf{k}\, \phi\left(\mathbf{k}-\frac{1}{2}\mathbf{p}'\right) \\
&\times \frac{1}{W - E_N(\mathbf{q}) - E_c(\mathbf{q}-\mathbf{k}) - E_c(\mathbf{k}) + i\epsilon} \\
&\times \sqrt{\frac{E_c(\mathbf{k})+m_c}{2E_c(\mathbf{k})}}\sqrt{\frac{E_c(\mathbf{q}-\mathbf{k})+m_c}{2E_c(\mathbf{q}-\mathbf{k})}} \\
&\times \left\{1 - \frac{\mathbf{k}\cdot(\mathbf{q}-\mathbf{k})}{[E_c(\mathbf{k})+m_c][E_c(\mathbf{q}-\mathbf{k})+m_c]}\right\}.
\end{aligned} \tag{29}$$

3. Final-state interactions

Including the final-state interaction, as illustrated in Fig. 6, the matrix element of the total amplitude in Eq. (12) is

$$\begin{aligned}
\langle \mathbf{p}' m_V m_s' | T_{VN,\gamma N}(W) | \mathbf{q}\lambda m_s\rangle = &\langle \mathbf{p}' m_V m_s' \,|\, B_{VN,\gamma N}(W) \,|\, \mathbf{q}\lambda m_s\rangle \\
&+ \langle \mathbf{p}' m_V m_s' | T^{(\mathrm{fsi})}_{VN,\gamma N} | \mathbf{q}(W)\lambda m_s\rangle\,,
\end{aligned} \tag{30}$$

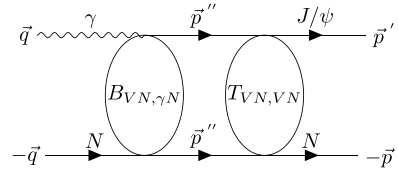

FIG. 6. J/ψ photoproduction on the nucleon with final-state interaction given in Eq. (31).

with

$$\begin{aligned}
&\langle \mathbf{p}' m_V m_s' \,|\, T^{(\mathrm{fsi})}_{VN,\gamma N}(W) \,|\, \mathbf{q}\lambda m_s\rangle \\
&= \sum_{m_V'',m_s''} \int d\mathbf{p}'' \langle \mathbf{p}\, m_V m_s' \,|\, T_{VN,VN}(W) \,|\, \mathbf{p}'' m_V'', m_s''\rangle \\
&\quad \times \frac{1}{W - E_N(p'') - E_V(p'') + i\epsilon} \\
&\quad \times \langle \mathbf{p}'' m_V'' m_s'' \,|\, B_{VN,\gamma N}(W) \,|\, \mathbf{q}\lambda, m_s\rangle.
\end{aligned} \tag{31}$$

With the spin-independent quark-N potential defined by Eq. (16), the $V+N\to V+N$ scattering amplitude in the above equation can be written as

$$\begin{aligned}
&\langle \mathbf{p}\, m_V m_s \,|\, T_{VN,VN}(W) \,|\, \mathbf{p}'\, m_V' m_s'\rangle \\
&\quad = \delta_{m_V,m_V'}\delta_{m_s,m_s'}\langle \mathbf{p}' \,|\, T_{VN}(W) \,|\, \mathbf{p}\rangle,
\end{aligned} \tag{32}$$

where $\langle \mathbf{p}'|T_{VN}(W)|\mathbf{p}\rangle$ is defined by the following Lippmann-Schwinger equation, as illustrated in Fig. 7:

$$\begin{aligned}
\langle \mathbf{p}'|T_{VN}(W)|\mathbf{p}\rangle = &\langle \mathbf{p}'|V_{VN}|\mathbf{p}\rangle \\
&+ \int d\mathbf{p}'' \frac{\langle \mathbf{p}'|V_{VN}|\mathbf{p}''\rangle\, \langle \mathbf{p}''|T_{VN}(W)|\mathbf{p}\rangle}{W - E_N(p'') - E_V(p'') + i\epsilon}.
\end{aligned} \tag{33}$$

Here $\langle \mathbf{p}'|V_{VN}|\mathbf{p}\rangle$ has been defined by Eq. (24).

We solve Eq. (33) in the partial-wave representation by using the following expansions:

$$\langle \mathbf{p}'|V_{VN}|\mathbf{p}\rangle = \sum_L \frac{2L+1}{4\pi} V_L(p', p) P_L(x), \tag{34}$$

and

$$\langle \mathbf{p}'|T_{VN}(W)|\mathbf{p}\rangle = \sum_L \frac{2L+1}{4\pi} T_L(p', p, W) P_L(x), \tag{35}$$

where $x = \hat{\mathbf{p}}\cdot\hat{\mathbf{p}}'$ and $P_L(x)$ is the Legendre function of the first kind. With Eq. (34) together with $\langle \mathbf{p}'|V_{VN}(W)|\mathbf{p}\rangle$ defined in Eq. (24), the partial-wave matrix element of potential can

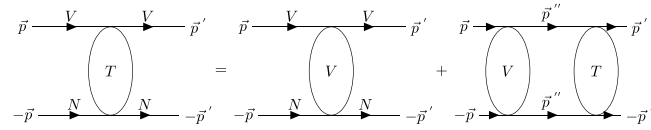

FIG. 7. The VN scattering equation defined by Eq. (33).

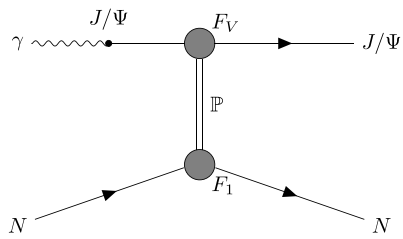

FIG. 8. The Pomeron-exchange model of Donnachie and Landshoff [26] for the $\gamma + N \to J/\psi + N$ reaction.

be calculated by

$$V_L(p', p) = (2\pi) \int_{-1}^{+1} dx P_L(x) \langle \mathbf{p}' | V_{VN} | \mathbf{p} \rangle , \tag{36}$$

If we set $F_V(\mathbf{t}) = 1$ in Eq. (24) and use Eq. (23) for a Yukawa form of the c-N potential $v_{cN}(r) = \alpha \frac{e^{-\mu r}}{r}$, one finds

$$V_L(p', p) = \frac{2}{\pi} \left(\frac{\alpha}{2pp'} \right) Q_L(Z), \tag{37}$$

where $Z = \frac{p^2+p'^2+\mu^2}{2pp'}$ and $Q_L(Z)$ is the Legendre function of the second kind.

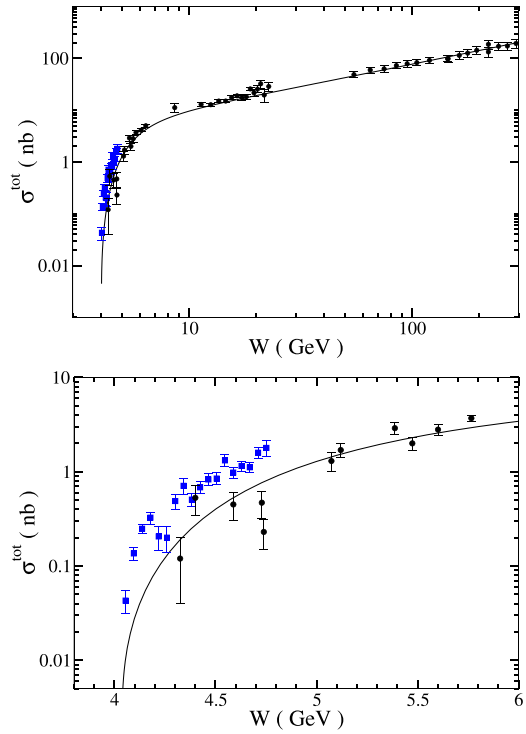

FIG. 9. Total cross sections from Pomeron-exchange amplitude for two different energy ranges: $4 \leqslant W \leqslant 300$ GeV (top) and for $4 \leqslant W \leqslant 6$ GeV (bottom). Data are taken from [31,32] (black circles) and [24] (blue squares), respectively.

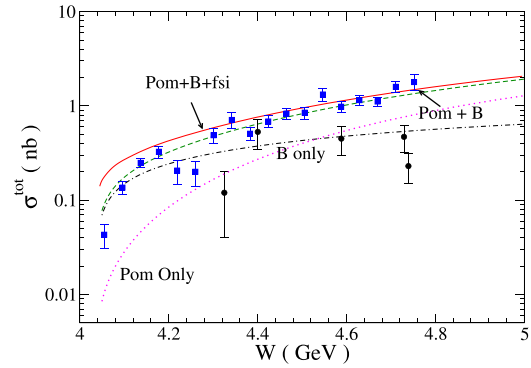

FIG. 10. Total cross sections for $4 \leqslant W \leqslant 5$ GeV from the 1Y model. The same data points are used as in Fig. 9.

By using Eqs. (34) and (35), Eq. (33) then leads to

$$T_L(p', p, W) = V_L(p', p) + \int dp'' p''^2 \Big[V_L(p', p'') \times \frac{1}{W - E_N(p'') + E_V(p'') + i\epsilon} \times T_L(p'', p, W) \Big]. \tag{38}$$

We solve Eq. (38) by using the standard numerical method described in Ref. [52]. The scattering phase shifts δ_L are calculated from the resulting $T_L(p'', p, W)$ as follows:

$$e^{i\delta_L} \sin\delta_L = -\pi \frac{p_0 E_N(p_0) E_V(p_0)}{E_N(p_0) + E_V(p_0)} T_L(p_0, p_0, W), \tag{39}$$

where p_0 represents the on-shell momentum and the invariant mass $W = E_N(p_0) + E_V(p_0)$. We will also calculate the scattering length a, which is defined for the $L = 0$ partial-wave at $p_0 \to 0$ as:

$$p_0 \cot\delta_0 = \frac{-1}{a}. \tag{40}$$

B. Pomeron-exchange amplitude $T^{\text{Pom}}_{VN,\gamma N}(W)$

Following the approach of Donnachie and Landshoff [26,53–55], the Pomeron-exchange amplitude is constructed within Regge phenomenology and is of the following:

$$\langle \mathbf{k}, m_V m'_s | T^{\text{Pom}}_{VN,\gamma N}(W) | \mathbf{q}, \lambda_\gamma m_s \rangle = \frac{1}{(2\pi)^3} \sqrt{\frac{m_N m_N}{4E_V(\mathbf{k}) E_N(\mathbf{p}') |\mathbf{q}| E_N(\mathbf{p})}} \times \left[\bar{u}(p', m'_s) \epsilon^*_\mu(k, \lambda_V) \mathcal{M}^{\mu\nu}_{\mathbb{P}}(k, p', q, p) \times \epsilon_\nu(q, \lambda_\gamma) u(p, m_s) \right]. \tag{41}$$

In this approach, the incoming photon is converted to a vector meson which is then scattered from the nucleon by the Pomeron-exchange mechanism, as illustrated in Fig. 8. The amplitude $\mathcal{M}^{\mu\nu}_{\mathbb{P}}(k, p', q, p)$ is given by

$$\mathcal{M}^{\mu\nu}_{\mathbb{P}}(k, p', q, p) = G_{\mathbb{P}}(s, t) \mathcal{T}^{\mu\nu}_{\mathbb{P}}(k, p', q, p), \tag{42}$$

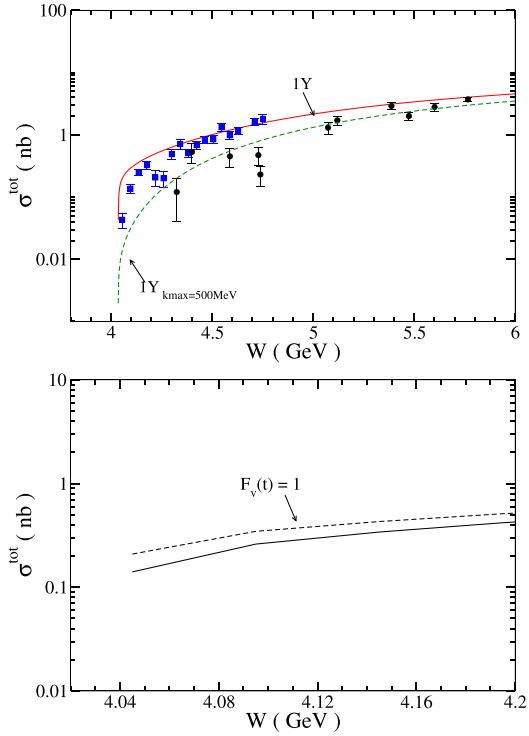

FIG. 11. The effect of the momentum cutoff $k_{\max} = 500$ MeV (top), and the effect of the form factor $F_V(t)$ (bottom), on the total cross section. The same data points are used as in Fig. 9.

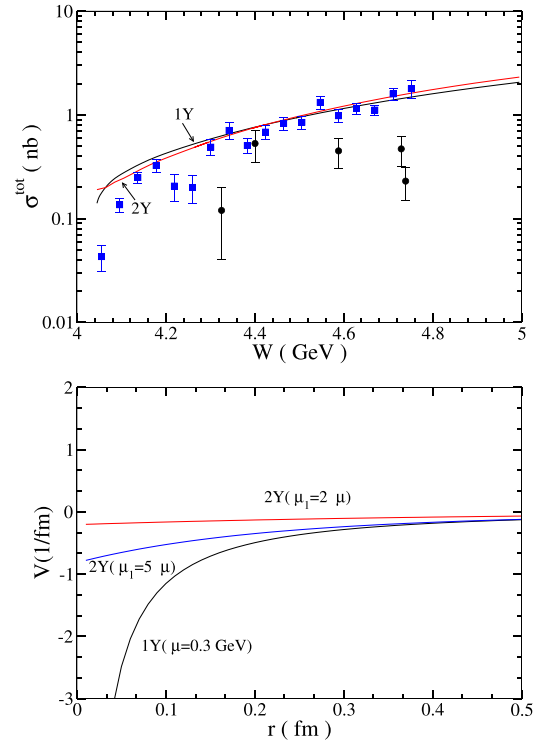

FIG. 12. Top panel: Total cross sections from 1Y model, and 2Y model. Bottom panel: Short-range behavior of $v_{cN}(r)$ for the 1Y and 2Y models. The same data points are used as in Fig. 9.

and

$$\mathcal{T}^{\mu\nu}_{\mathbb{P}}(k, p', q, p) = i\,2\frac{e\,m_V^2}{f_V}[2\beta_{q_V}F_V(t)][3\beta_{u/d}F_1(t)] \times \{\not{q}g^{\mu\nu} - q^\mu\gamma^\nu\}, \tag{43}$$

where m_V is the mass of the vector meson and $f_V = 5.3$, 15.2, 13.4, 11.2, 40.53 for $V = \rho, \omega, \phi, J/\psi, \Upsilon$ are traditionally determined by the widths of the $V \to \gamma \to e^+e^-$ decays. The parameters β_{q_V} ($\beta_{u/d}$) define the coupling of the Pomeron with the quark q_V (u or d) in the vector meson V (the nucleon N). In Eq. (43), a form factor for the Pomeron-vector meson vertex is also introduced with

$$F_V(t) = \frac{1}{m_V^2 - t}\left(\frac{2\mu_0^2}{2\mu_0^2 + m_V^2 - t}\right), \tag{44}$$

where $t = (q-k)^2 = (p-p')^2$. By using the Pomeron-photon analogy, the form factor for the Pomeron-nucleon vertex is defined by the isoscalar electromagnetic form factor of the nucleon as follows:

$$F_1(t) = \frac{4m_N^2 - 2.8t}{(4m_N^2 - t)(1 - t/0.71)^2}. \tag{45}$$

Here t is in the unit of GeV^2 and m_N is the proton mass.

The propagator $G_{\mathbb{P}}$ of the Pomeron in Eq. (42) follows the Regge phenomenology form:

$$G_{\mathbb{P}} = \left(\frac{s}{s_0}\right)^{\alpha_P(t)-1}\exp\left\{-\frac{i\pi}{2}[\alpha_P(t) - 1]\right\}, \tag{46}$$

where $s = (q+p)^2 = W^2$, $\alpha_P(t) = \alpha_0 + \alpha'_P t$, and $s_0 = 1/\alpha'_P$. We use the value of $s_0 = 0.25$ GeV from the works [26,53–55] of Donnachie and Landshoff.

$T^{\text{Pom}}_{VN,\gamma N}(W)$ has been determined in Refs. [1,56,57] by fitting the data of total cross sections up to 300 GeV. The resulting parameters for ρ^0, ω, ϕ photoproduction [58] have been determined as follows: $\mu_0 = 1.1$ GeV^2, $\beta_{u/d} = 2.07$ GeV^{-1}, $\beta_s = 1.38$ GeV^{-1}, $\alpha_0 = 1.08$ for ρ and ω, and $\alpha_0 = 1.12$ for ϕ. For the heavy quark systems, we find that using the same μ_0^2, $\beta_{u/d}$, and α'_P values, the photoproduction data for J/ψ and Υ can be fitted by setting $\beta_c = 0.32$ GeV^{-1} and $\beta_b = 0.45$ GeV^{-1}, along with a larger $\alpha_0 = 1.25$.

Figure 9 depicts the total cross section for the J/ψ photoproduction on the nucleon obtained solely from the contribution of the Pomeron-exchange amplitude and compares it with the data from Refs. [23,24][1] and [31,32]. One can see from Fig. 9 that while the Pomeron-exchange mechanism effectively describes the data (black circles) [31,32] at very high energies, it falls short in accurately describing the the data (blue squares) [23,24] from the GlueX experiment at JLab.

[1]To make clearer comparisons, this analysis includes only the latest total cross-section data with higher statistics from Ref. [24].

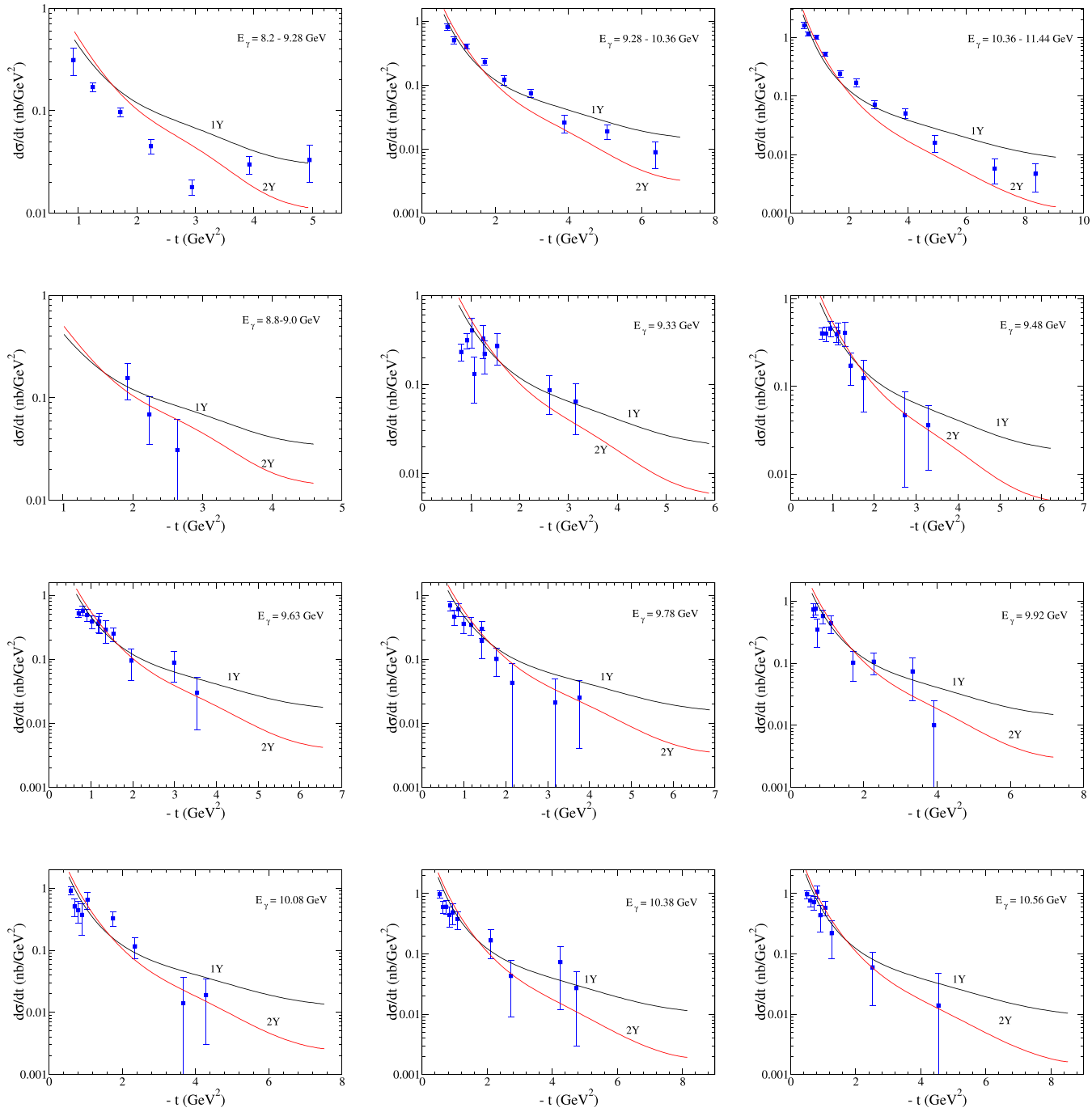

FIG. 13. Differential cross sections from the 1Y model and 2Y model. The data in the top three panels are taken from the GlueX Collaboration [24]. The other data are taken from an experiment at JLab's Hall-C [25].

III. RESULTS

A. Determination of quark-nucleon potential v_{cN}

We are guided by the Yukawa form of J/ψ-N potential extracted from the LQCD calculation of Ref. [18] to determine the quark-N potential v_{cN}. We observe that the factorized form of $V_{VN,VN}$ in Eq. (24) suggests that if $v_{cN}(r)$ is also in the Yukawa form, the resulting $V_{VN,VN}$ can approach the J/ψ-N potential of Ref. [18] at large distance r. We therefore consider the following parametrization:

$$v_{cN}(r) = \alpha\left(\frac{-\mu r}{r} - c_s\frac{e^{-\mu_1 r}}{r}\right). \tag{47}$$

We first consider a model (1Y) with $c_s = 0$, meaning that the resulting J/ψ-N potential takes on the Yukawa form extracted from LQCD. The calculation then only has two free parameters, α and μ. We find that the total cross-section data

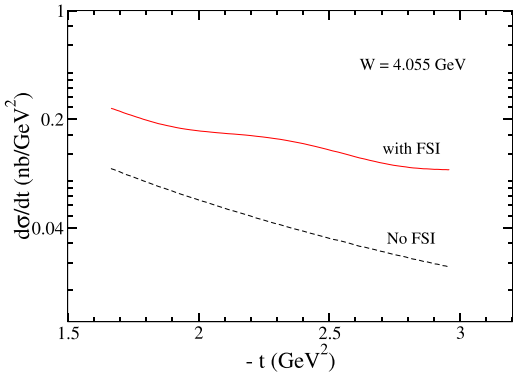

FIG. 14. Prediction of the differential cross sections near threshold at $W = 4.055$ GeV by using 2Y model.

[23,24] from JLab for the small W region can be best fitted by choosing $\alpha = -0.067$ and $\mu = 0.3$ GeV if the J/ψ wave function is taken from the CQM model of Ref. [46]. We show in Fig. 10 the total cross sections for the J/ψ photoproduction in the small $4 \leqslant W \leqslant 5$ GeV region obtained from the 1Y model. The dotted, dot-dashed, and dashed lines represent the results obtained from the Pomeron-exchange, Born term, and the sum of Pomeron-exchange and Born term contributions, respectively. The solid line represents the full result, including the final-state interaction in addition to the Pomeron-exchange and Born terms. As seen in Fig. 10, the Pomeron-exchange mechanism alone is insufficient to fit the JLab data [23,24], particularly for low-energy regimes. However, the contribution from the c-N interaction v_{cN} is essential for fitting the data in this 1Y model. In particular, the cross sections in

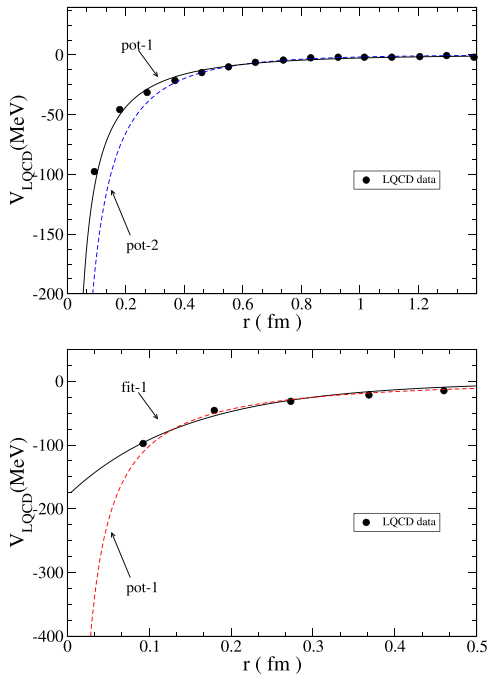

FIG. 15. Two different forms of J/ψ-N potential $V^{\mathrm{LQCD}}(r)$: $\alpha_L \frac{e^{-\mu_L r}}{r}$ (top panel) and $\alpha_L(\frac{e^{-\mu_L r}}{r} - \frac{e^{-N_L \mu_L r}}{r})$ (bottom panel), obtained from fitting the LQCD data [18,20].

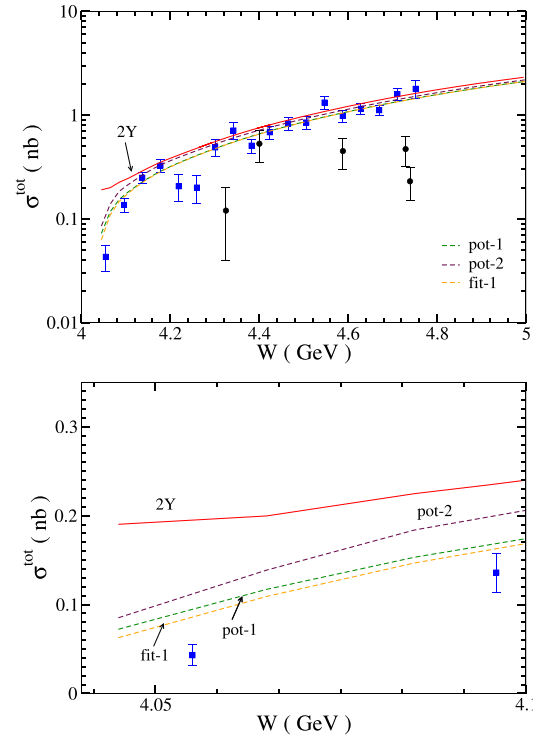

FIG. 16. Total cross sections of J/ψ calculated from the three models pot-1, pot-2, and fit-1 constrained by the LQCD data. Top panel: For $4 \leqslant W \leqslant 5$ GeV. Bottom panel: For the near threshold region. The same data points are used as in Fig. 9.

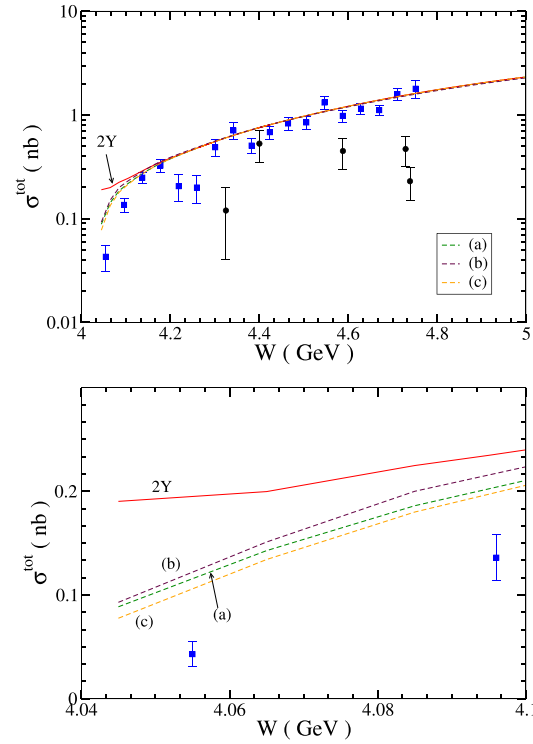

FIG. 17. Total cross sections calculated from the three models (a), (b), and (c) constrained by the LQCD data. Top panel: For $4 \leqslant W \leqslant 5$ GeV. Bottom panel: For the near threshold region. The same data points are used as in Fig. 9.

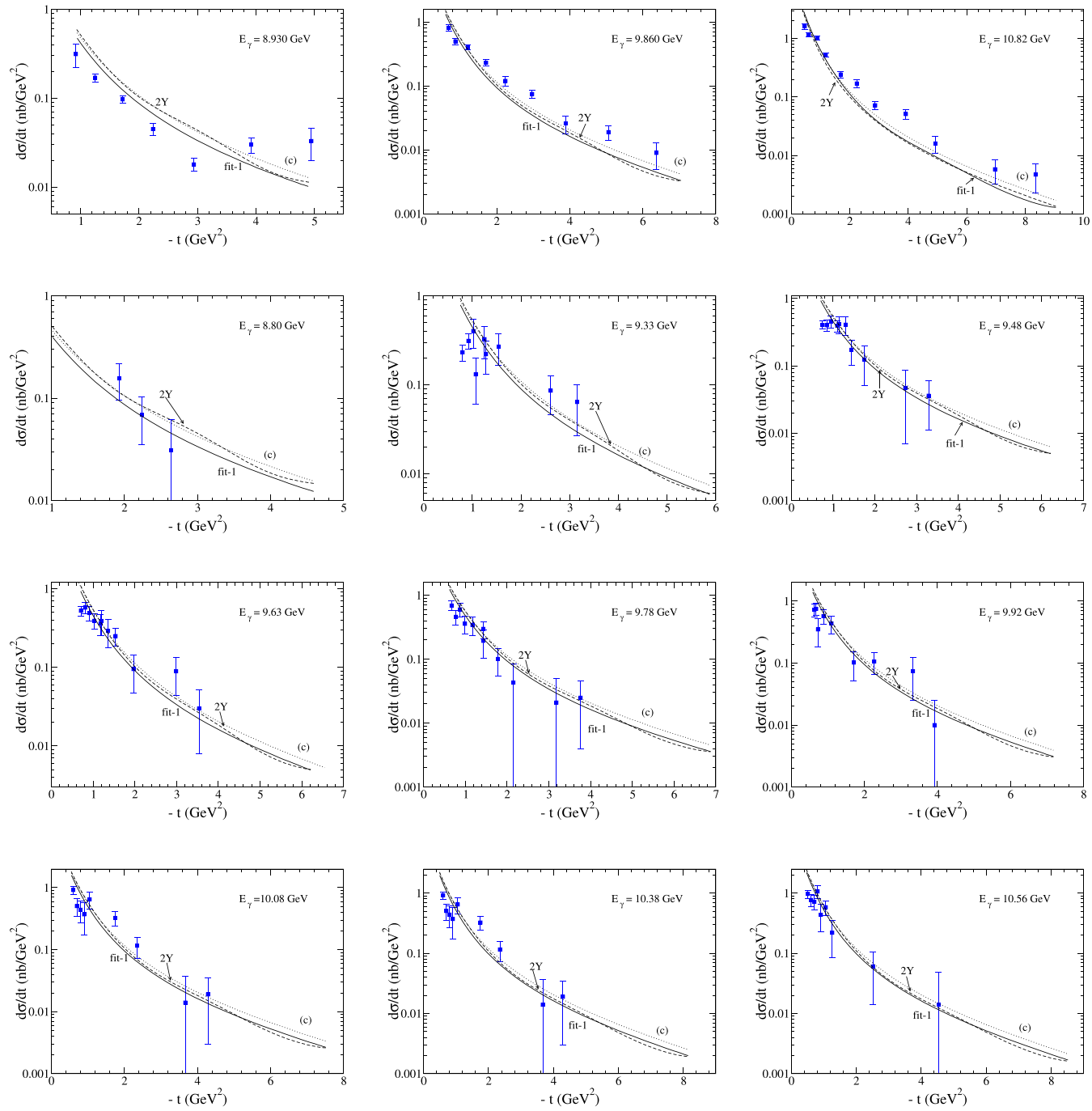

FIG. 18. Differential cross sections from the models 2Y, fit-1, and (c). The data in the top three panels are taken from the GlueX Collaboration [24]. The other data are taken from an experiment at JLab's Hall-C [25].

the very near threshold region are largely determined by the FSI term. These results demonstrate that J/ψ-N interactions can be extracted rather clearly from the J/ψ photoproduction data within this model, which does not use the VMD assumption. More importantly, the calculations properly account for off-shell effects and satisfy the unitarity condition, a feature that is not considered in most, if not all, previous approaches discussed in Ref. [1].

To see the importance of using a realistic J/ψ wave function, we compare the cross section from the full calculation and that from using a wave function that employs a momentum cutoff in evaluating $B_{VN,\gamma N}$ amplitude. Specifically, we replace the integral $B = \int_0^\infty \phi(k)(\cdots)dk$ with $\int_0^{k_{\rm max}} \phi(k)(\cdots)dk$ to evaluate the cut-off effect.

In the top panel of Fig. 11, we illustrate the impact of the momentum cutoff $k_{\rm max}$ on the total cross section. The solid line represents the result obtained without the cutoff (i.e., $k_{\rm max} \to \infty$), while the dashed line corresponds to the result obtained with the cut-off value of $k_{\rm max} = 500$ MeV.

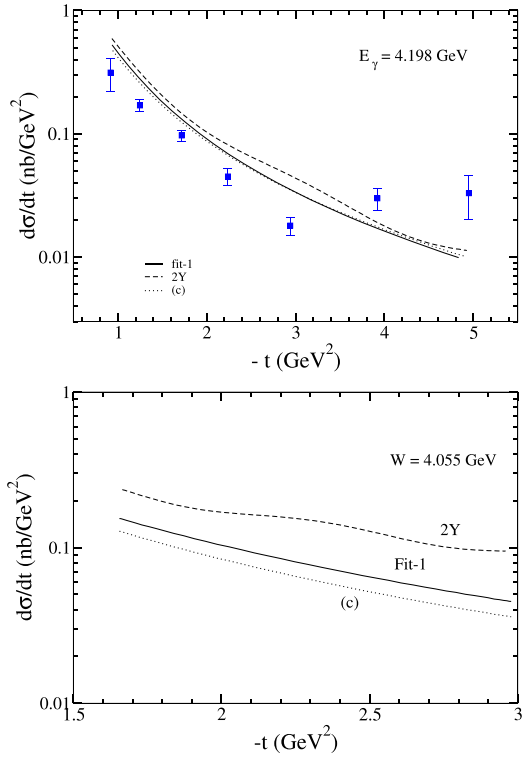

FIG. 19. Differential cross sections obtained from each model listed in Table I. The data are taken from Ref. [25].

Clearly, the high momentum tail of the J/ψ wave function is crucial for fitting the data, particularly the JLab data [23,24] in the low-energy region. We also note that using the Gaussian wave function determined by $J/\psi \to e^+e^-$ of Ref. [1] results in much larger cross sections, and fitting to the JLab data requires a much smaller value of α.

As one can see from Eq. (24), the J/ψ-N potential is determined by the form factor $F_V(t)$, which is obtained from the convolution of the initial and final-state J/ψ wave functions. In the bottom panel of Fig. 11, we illustrate the impact of $F_V(t)$ on the total cross section by comparing the results from including the momentum-dependent form factor $F_V(t)$ (solid line) and setting $F_V(t) = 1$ (dashed line). It is evident that the effect of $F_V(t)$ on the total cross section is significant, underscoring the importance of using a realistic J/ψ wave function in determining the J/ψ-N interaction and the FSI effects.

B. The 2Y model

We now consider the model ($2Y$) by incorporating the second term with $c_s = 1$ in addition to the first term in Eq. (47). The cutoff of the short-range part is set as $\mu_1 = N\mu$. We observe that for large values of $N > 50$, the 2Y model closely approximates the 1Y model, and the JLab data can be fitted with any $N < 20$ by adjusting the coupling constant α. The result of the total cross section from the 2Y model with $N = 5$ and $\alpha = -0.145$ is comparable to that of the 1Y model with $\alpha = -0.067$, as shown in the top panel of Fig. 12. The two models fit the JLab data [24,25] equally well but have very large difference at very near threshold, which is dominated completely by FSI. The origin of it is that they have very different short range behaviors of the potentials $v_{cN}(r)$, as shown in the bottom panel.[2] We thus expect that their predictions on the differential cross sections must be large at large t. This is shown in Fig. 13, where the differential cross sections as a function of t from the 1Y model with $\alpha = -0.067$ and the 2Y model with $\alpha = -0.145$ and $N = 5$ are compared. Both models reasonably describe the JLab data from the GlueX Collaboration [24] and Hall-C [25]. We observe notable differences between the predictions of the 1Y and 2Y models at large values of t. More precise data are clearly needed for making further progress, while the 2Y model appears to be better. For future experiments at very near threshold, we present in Fig. 14 the differential cross sections at $W = 4.055$ GeV. We compare the predictions of the 2Y model with (solid line) and without (dashed line) including the FSI.

C. LQCD constraints

We have found that the J/ψ-N potentials resulting from fitting the JLab data in the previous section give the J/ψ-N scattering lengths, $-a \approx 0.3$–0.7 fm, which are rather different from those extracted from the LQCD data of Ref. [18]. Thus, it raises the question of our parametrization of the quark-N potential $v_{cN}(r)$. At low energies, the J/ψ-N system has a small relative momentum, and the multigluon exchange involving two quarks in J/ψ may play important roles. Therefore, we need to extend our parametrization of v_{cN} to include two-body operator. However, we will not explore this possibility in this exploratory work because the model would then have too many parameters, which cannot be determined by the still very limited data in the near threshold region. Instead, we next consider the models constructed by imposing LQCD constraints on the calculations of the FSI. This is done by using the LQCD data of Refs. [18,20] to determine the parameters of $v_{cN}(r)$ in calculating the matrix elements of the J/ψ-N potential $V_{VN,VN}$ defined by Eqs. (19)–(22), while the Born term amplitude $B_{\gamma N,VN}$ from the 2Y model described in the previous section is kept in the calculations. This allows us to investigate the extent to which the extracted J/ψ-N scattering amplitudes can be related to the LQCD data of Refs. [18,20].

The LQCD data of Ref. [20] for the J/ψ-N potential have large uncertainties at small distances r. Therefore, we fit the LQCD data for the region of large r using the following form of J/ψ-N potential: $V^{\rm LQCD}(r) = \alpha_L \frac{e^{-\mu_L r}}{r}$ with two different sets of parameters (α_L, μ_L), namely $(\alpha_L, \mu_L) = (-0.06, 0.3)$ and $(-0.11, 0.5)$, which we denote as "pot-1" and "pot-2," respectively.

The results of $V^{\rm LQCD}(r) = \alpha_L \frac{e^{-\mu_L r}}{r}$ obtained from the "pot-1" and "pot-2" are shown in the upper panel of Fig. 15. As one can see from the figure, their short-range parts are rather

[2]To compare the potential for the 1Y model (black line), we evaluate for the 2Y model with $N = 2$ (red line) and $N = 5$ (blue line), using the same $\alpha = -0.145$ for both N values. This ensures clear comparisons of their r dependence at short distances.

TABLE I. The parameters for the models (a), (b), and (c) imposing LQCD constraints on FSI.

Model	$\alpha_{\rm FSI}$	μ (GeV)	μ_1 (GeV)	a (fm)	α_B
(a)	−0.03	0.3	—	−0.15	−0.162
(b)	−0.055	0.5	—	−0.233	−0.152
(c)	−0.1	0.9	1.8	−0.057	−0.163

different, while their long-range parts (i.e., $r \geqslant 0.6$ fm) are almost similar. Following the derivations of Eqs. (20)–(25), one can see that the matrix element of $V^{\rm LQCD}(r)$ is of the form of Eq. (24) with $F_V(t) = 1$ and $v_{cN}(r)$ calculated from the 1Y model, i.e., $v_{cN}(r) = \alpha \frac{e^{-\mu r}}{r}$ with $\alpha = 1/2\alpha_L$ and $\mu = \mu_L$. Thus, the parameters of $v_{cN}(r)$ for this FSI calculation are $(\alpha \equiv \alpha_{\rm FSI} = \alpha_{\rm L}/2, \mu \equiv \mu_L) = (-0.03, 0.3)$ fixed from "pot-1" and $(-0.055, 0.5)$ fixed from "pot-2."

In the lower panel of Fig. 15, we also fit the LQCD data using another form of J/ψ-N potential, $V^{\rm LQCD}(r) = \alpha_L(\frac{e^{-\mu_L r}}{r} - \frac{e^{-N_L \mu_L r}}{r})$ with $(\alpha_L, \mu_L, N_L) = (-0.2, 0.3, 2)$, which we denote as "fit-1" and compare it with the result of "pot-1." The result of "fit-1" has a rather different short range behavior compared with that of "pot-1." The FSI calculation with this potential can then be done by using the 2Y model of $v_{cN}(r) = \alpha(\frac{e^{-\mu r}}{r} - \frac{e^{-N\mu r}}{r})$ to evaluate Eq. (24) with $F_V(t) = 1$ and $(\alpha \equiv \alpha_{\rm FSI} = \alpha_{\rm L}/2, \mu \equiv \mu_L, N \equiv N) = (-0.1, 0.3, 2)$.

With the three J/Ψ-N potentials, i.e., pot-1, pot-2, and fit-1, we then have three models. They have the same Born term $B_{\gamma N,VN}(E)$ from the 2Y model of the previous section, but their FSI amplitude $T^{\rm (fsi)}_{\gamma N,VN}$ defined in Eq. (31) are different because the $VN \to VN$ amplitude $T_{VN,VN}$ depends on the chosen J/ψ-N potential. The resulting total cross sections are presented in Fig. 16 for $4 \leqslant W \leqslant 5$ (GeV) region (top) and for the near threshold region (bottom), respectively. For comparison, we also show the result obtained from the 2Y model of the previous section. As depicted in the top panel of Fig. 16, no large difference is observed between the models with LQCD constraints and the 2Y model in the higher-energy region $W \geqslant 4.2$-GeV region. However, as illustrated in the bottom panel, the 2Y model predicts a much larger cross section in the very near threshold region $W \leqslant 4.1$ GeV. These results suggest that imposing the LQCD constraints significantly changes the threshold behavior and the predicted cross sections are closer to the JLab data [23,24] than the 2Y model.

As illustrated in Fig. 14, we see that the cross sections near the threshold shown in the lower panel of Fig. 16 are mainly due to the FSI term $T^{\rm (fsi)}_{\gamma N,VN}$ given by Eq. (31), which depends on both the Born amplitude $B_{\gamma N,VN}$ and the $VN \to VN$ amplitude $T_{VN,VN}$. Thus, the large difference between 2Y and three models with the LQCD constraints could be reduced if each model's Born term is refined to fit the data at higher energies as well as the 2Y model. To examine this model dependence of our predictions, we next construct three models by modifying the parameter $\alpha \to \alpha_B$ of the quark-nucleon potential $v_{cN}(r)$ used in the calculation of the Born term $B_{\gamma N,VN}$ to fit the total cross sections from the 2Y model for $W \geqslant 4.1$ GeV. We denote the resulting models as (a), (b), and (c) for the models pot-1, pot-2, and fit-1, respectively. The determined

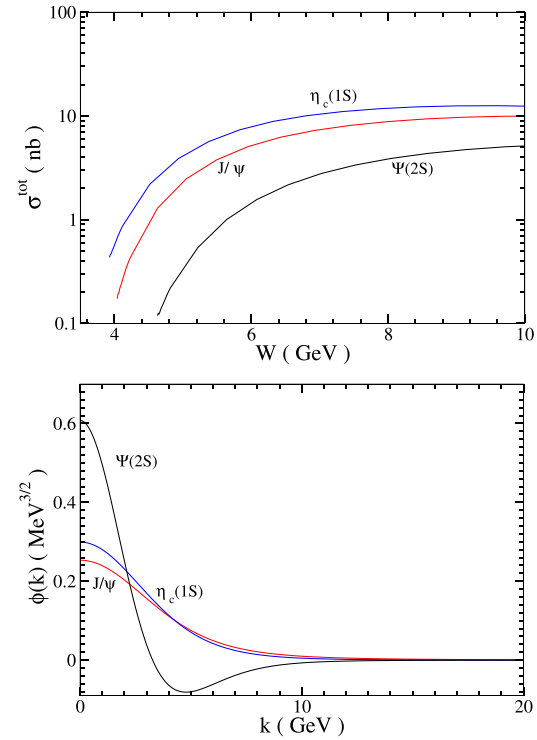

FIG. 20. Top pandel: Predicted total cross sections of $\eta_c(1S)$ and $\psi(2S)$ photoproduction, Bottom panel: The wave functions of J/ψ, $\eta_c(1S)$, and $\psi(2S)$.

parameter α_B along with the other parameters of the three models are listed in Table I. Note that the scattering length a is calculated solely from the $VN \to VN$ amplitude $T_{VN,VN}(W)$. Our predictions for a obtained from models (a), (b), and (c) are $(-0.15, -0.233, -0.057)$ fm, respectively, while we obtain $a = -0.67$ fm from the 2Y model. These different scattering lengths are related to the differences in the total cross sections between the four models. It will be interesting to have data to distinguish these predictions and test LQCD. This would allow for a comparison between the predicted scattering lengths and the actual experimental results.

Using the model parameters listed in Table I, we obtain the total cross sections shown in Fig. 17. They are almost indistinguishable at high W, while their differences with the 2Y model at near threshold energy are large and comparable to that shown in Fig. 16. Thus, our predictions near threshold are rather robust for future experimental tests. We also find that the differential cross sections from all models with LQCD constraints, as given above, can describe the available data of differential cross sections as well as the 2Y model. This is illustrated in Fig. 18 for the model fit-1 and (c). For future measurements at energies very close to the threshold, we present predicted differential cross sections in Fig. 19.

D. Photoproduction of $\eta_c(1S)$ and $\psi(2S)$

With the parameters of v_{cN} determined from fitting the JLab data [23–25], we proceed to predict the photoproduction of $\eta_c(1S)$ and $\psi(2s)$ mesons. Because v_{cN} is spin independent and the wave functions for $\eta_c(1S)$ and $\psi(2S)$ are also of the

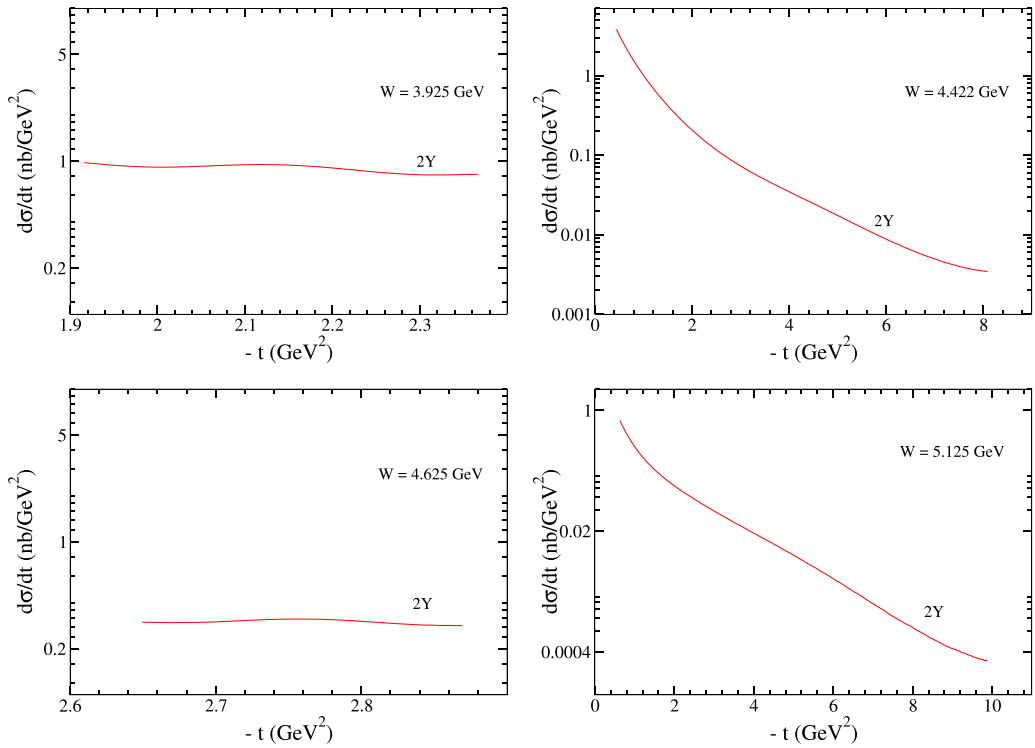

FIG. 21. Top two panels: Predicted differential cross sections of $eta_c(1S)$ photoproduction at 20 MeV (left) and 500 MeV (right) from threshold. Bottom two panels: Predicted differential cross sections of $eta_c(1S)$ at 20 MeV (left two panels) and 500 MeV (right two panels) from the thresholds.

s-wave form given by Eq. (9), the calculations can be done by using the same formula presented in Sec. III by simply changing the wave functions and the kinematics associated with the masses of mesons. By using the parameters of the 2Y model presented in the previous section, the predicted total cross sections for the photoproductions of $\eta_c(1S)$, $\psi(2s)$, and J/ψ are presented in the top panel of Fig. 20, along with the comparison of their wave functions in the bottom panel. In Fig. 21, we present the predicted differential cross sections for $\eta_c(1S)$ (upper panels) and $\psi(2S)$(lower panels) at energies 20 MeV (left) and 500 MeV (right) above the thresholds.

As a validation test for our model, it would be intriguing to compare our predictions with forthcoming data expected from experiments at JLab and the future EIC.

IV. SUMMARY AND FUTURE IMPROVEMENTS

Within a Hamiltonian formulation [27–30], a dynamical model based on the CQM and a phenomenological charm quark-nucleon potential $v_{cN}(r)$ is constructed to investigate the J/ψ photoproduction on the nucleon at energies near threshold. The main feature of the model lies in the quark-N potential, v_{cN}, which generates a photoproduction amplitude defined by a $c\bar{c}$-loop integration over the $\gamma \to c\bar{c}$ vertex function and the J/ψ wave function, $\phi_{J/\psi}(c\bar{c})$, from the CQM described in Ref. [46]. In addition, the J/ψ-N final-state interaction is calculated from a J/ψ-nucleon potential $V_{J/\psi N}(r)$, which is constructed by folding $v_{cN}(r)$ into the same wave function $\phi_{J/\psi}(c\bar{c})$. By also incorporating the Pomeron-exchange amplitudes determined in Refs. [1,57], the constructed model can describe the available data from threshold to high energies, up to the invariant mass $W = 300$ GeV.

The parametrization of $v_{cN}(r)$ is chosen such that the constructed $V_{J/\psi N}(r)$ at large distances has the same Yukawa potential form extracted from a LQCD calculation. The parameters of v_{cN} are determined by fitting the total cross-section data of JLab [23,24] by performing calculations that include J/ψ-N final-state interactions, as required by the unitarity condition. The predicted differential cross sections $d\sigma/dt$ are in reasonably good agreement with the data from JLab [24,25]. Furthermore, it is shown that the FSI effects dominate the cross section in the very near-threshold region. This indicates that the low-energy J/ψ-N scattering amplitudes and the associated models of J/ψ-N potentials $V_{J/\psi N}(r)$ can be extracted from the J/ψ photoproduction data with high sensitivity. The determined $V_{J/\psi N}(r)$ can be used to understand the nucleon resonances $N^*(P_c)$ reported by the LHCb collaboration [2–5], to extract the gluonic distributions in nuclei, J/ψ production in relativistic heavy-ion collisions, and to study the existence of nuclei with hidden charms [6–10].

By imposing the constraints of J/ψ-N potential extracted from the LQCD calculation of Refs. [18–20], we have obtained three J/ψ-N potentials which fit the JLab data equally well. The resulting J/ψ-N scattering lengths are in the range of $a = [-0.05, -0.25]$ fm, which rule out the existence of free J/ψ-N bound states. On the other hand, the available data near threshold is far from sufficient to draw a conclusion. Clearly, more extensive and precise experimental data are needed to make further progress.

With the determined quark-nucleon potential $v_{cN}(r)$ and the wave functions generated from the same CQM of Ref. [46], the constructed dynamical model has been used to predict the cross sections of photoproduction of $\eta_c(1S)$ and $\psi(2S)$ mesons. It will be interesting to have data from experiments at JLab and EIC to test our predictions.

The model presented here needs to be improved in the future. Our parametrization of quark-nucleon potential v_{cN} is guided by the Yukawa form extracted from a LQCD calculation of Ref. [18]. This must be improved by using more advanced LQCD calculations of J/ψ-N scattering, in particular the short-range part of the potential. A recent LQCD calculation of ϕ-N interaction leads to a more complex form than the simple Yukawa form. In addition, the quark substructure of the nucleon must be considered in the future improvements of our model as well as most, if not all, of the previous models (as reviewed in Ref. [1]). However, this is a nontrival many-body problem similar to that encountered in the investigations of nuclear reactions [51].

The results from the model based on the effective Lagrangian approach [21] suggest that we need to extend our model to include the coupled-channel effects via the $\bar{D} * \Lambda_c$ channel in order to explain the cusp structure of the total cross-section data near $W \approx 4.2$–4.3 GeV. However, this improvement must also consider other coupled-channels effects arising from the coupling with πN and ρN channels, as investigated in Ref. [57].

It is necessary to improve our model by developing $c\bar{c}$-loop calculations of Pomeron-exchange mechanism, which are needed to fit the high-energy data. This requires an extension of our approach to include relativistic effects. This can be done straightforwardly within the instant form of relativistic quantum mechanics of Dirac [45], while the Light-front form is also possible with much more works.

ACKNOWLEDGMENTS

We thank J. Segovia for providing us with the CQM wave functions used in this work. The works of S.S and H.-M.C. were supported by the National Research Foundation of Korea (NRF) under Grant No. NRF- 2023R1A2C1004098. The work of T.-S.H.L. was supported by the U.S. Department of Energy, Office of Science, Office of Nuclear Physics, under Contract No. AC02-06CH11357.

[1] T.-S. H. Lee, S. Sakinah, and Y. Oh, Models of J/ψ photoproduction reactions on the nucleon, Eur. Phys. J. A **58**, 252 (2023).
[2] R. Aaij *et al.* (LHCb Collaboration), Observation of $J/\psi p$ resonances consistent with pentaquark states in $\Lambda_b^0 \to J/\psi K^- p$ decays, Phys. Rev. Lett. **115**, 072001 (2015).
[3] R. Aaij *et al.* (LHCb Collaboration), Evidence for exotic hadron contributions to $\Lambda_b^0 \to J/\psi p\pi^-$ decays, Phys. Rev. Lett. **117**, 082003 (2016).
[4] R. Aaij *et al.*, Observation of a narrow pentaquark state, $P_c(4312)^+$, and of the two-peak structure of the $P_c(4450)^+$, Phys. Rev. Lett. **122**, 222001 (2019).
[5] R. Aaij *et al.* (LHCb Collaboration), Evidence for a new structure in the $J/\psi p$ and $J/\psi \bar{p}$ systems in $B_s^0 \to J/\psi p\bar{p}$ decays, Phys. Rev. Lett. **128**, 062001 (2022).
[6] S. J. Brodsky and G. F. de Teramond, Spin correlations, QCD color transparency, and heavy-quark thresholds in proton-proton scattering, Phys. Rev. Lett. **60**, 1924 (1988).
[7] S. J. Brodsky, I. Schmidt, and G. F. de Teramond, Nuclear-bound quarkonium, Phys. Rev. Lett. **64**, 1011 (1990).
[8] H. Gao, T.-S. H. Lee, and V. Marinov, ϕ-N bound state, Phys. Rev. C **63**, 022201(R) (2001).
[9] V. B. Belyaev, N. V. Shevchenko, A. Fix, and W. Sandhas, Binding of charmonium with two- and three-body nuclei, Nucl. Phys. A **780**, 100 (2006).
[10] J.-J. Wu and T.-S. H. Lee, Photoproduction of bound states with hidden charm, Phys. Rev. C **86**, 065203 (2012).
[11] M. E. Peskin, Short-distance analysis for heavy-quark systems (I). Diagrammatics, Nucl. Phys. B **156**, 365 (1979).
[12] G. Bhanot and M. E. Peskin, Short-distance analysis for heavy-quark systems (II). Applications, Nucl. Phys. B **156**, 391 (1979).
[13] M. Luke, A. V. Manohar, and M. J. Savage, A QCD calculation of the interaction of quarkonium with nuclei, Phys. Lett. B **288**, 355 (1992).
[14] S. J. Brodsky and G. A. Miller, Is J/ψ-nucleon scattering dominated by the gluonic van der Waals interaction? Phys. Lett. B **412**, 125 (1997).
[15] A. B. Kaidalov and P. E. Volkovitsky, Heavy-quark interactions with nucleons and nuclei, Phys. Rev. Lett. **69**, 3155 (1992).
[16] N. Ishii, S. Aoki, and T. Hatsuda, Nuclear force from lattice QCD, Phys. Rev. Lett. **99**, 022001 (2007).
[17] S. Aoki, T. Hatsuda, and N. Ishii, Theoretical foundation of the nuclear force in QCD and its applications to central and tensor forces in quenched lattice QCD simulations, Prog. Theor. Phys. **123**, 89 (2010).
[18] T. Kawanai and S. Sasaki, Charmonium-nucleon potential from lattice QCD, Phys. Rev. D **82**, 091501(R) (2010).
[19] T. Kawanai and S. Sasaki, Charmonium-nucleon interaction from lattice QCD with $2+1$ flavors of dynamical quarks, AIP Conf. Proc. **1388**, 640 (2011).
[20] S. Sasaki (private communications, 2020).
[21] M. L. Du *et al.*, Deciphering the mechanism of near-threshold J/ψ photoproduction, Eur. Phys. J. C **80**, 1053 (2020).
[22] Y.-Z. Xu, S.-Y. Chen, Z.-Q. Yao, D. Binosi, Z.-F. Cui, and C. D. Roberts, Vector-meson production and vector meson dominance, Eur. Phys. J. C **81**, 895 (2021).
[23] A. Ali *et al.* (GlueX Collaboration), First measurement of near-threshold J/ψ exclusive photoproduction off the proton, Phys. Rev. Lett. **123**, 072001 (2019).
[24] S. Adhikari *et al.* (GlueX Collaboration), Measurement of the J/ψ photoproduction cross section over the full near-threshold kinematic region, Phys. Rev. C **108**, 025201 (2023).
[25] B. Duran *et al.*, Determining the gluonic gravitational form factors of the proton, Nature (London) **615**, 813 (2023).
[26] A. Donnachie and P. V. Landshoff, Elastic scattering and diffraction dissociation, Nucl. Phys. B **244**, 322 (1984).
[27] T. Sato and T.-S. H. Lee, Meson-exchange model for πN scattering and $\gamma N \to \pi N$ reaction, Phys. Rev. C **54**, 2660 (1996).

[28] A. Matsuyama, T. Sato, and T.-S. H. Lee, Dynamical coupled-channel model of meson production reactions in the nucleon resonance region, Phys. Rep. **439**, 193 (2007).
[29] B. Juliá-Díaz, T.-S. H. Lee, A. Matsuyama, and T. Sato, Dynamical coupled-channels model of πN scattering in the $W \leqslant 2$ GeV nucleon resonance region, Phys. Rev. C **76**, 065201 (2007).
[30] H. Kamano, S. X. Nakamura, T.-S. H. Lee, and T. Sato, Nucleon resonances within a dynamical coupled-channels model of πN and γN reactions, Phys. Rev. C **88**, 035209 (2013).
[31] M. Derrick *et al.* (ZEUS Collaboration), Measurement of the cross section for the reaction $\gamma p \to J/\psi p$ with the ZEUS detector at HERA, Phys. Lett. B **350**, 120 (1995).
[32] C. Adloff *et al.* (H1 Collaboration), Elastic photoproduction of J/ψ and Υ mesons at HERA, Phys. Lett. B **483**, 23 (2000).
[33] C. D. Roberts and A. G. Williams, Dyson–Schwinger equations and their application to hadronic physics, Prog. Part. Nucl. Phys. **33**, 477 (1994).
[34] C. D. Roberts, Electromagnetic pion form factor and neutral pion decay width, Nucl. Phys. A **605**, 475 (1996).
[35] M. A. Pichowsky and T.-S. H. Lee, Pomeron-exchange and exclusive electroproduction of ρ-mesons in QCD, Phys. Lett. B **379**, 1 (1996).
[36] M. A. Pichowsky and T.-S. H. Lee, Exclusive diffractive processes and the quark substructure of mesons, Phys. Rev. D **56**, 1644 (1997).
[37] P. Maris and C. D. Roberts, π- and K-meson Bethe-Salpeter amplitudes, Phys. Rev. C **56**, 3369 (1997).
[38] L. Chang, Y.-X. Liu, and C. D. Roberts, Dressed-quark anomalous magnetic moments, Phys. Rev. Lett. **106**, 072001 (2011).
[39] L. Chang, I. C. Cloët, C. D. Roberts, S. M. Schmidt, and P. C. Tandy, Pion electromagnetic form factor at spacelike momenta, Phys. Rev. Lett. **111**, 141802 (2013).
[40] S.-X. Qin and C. D. Roberts, Impressions of the continuum bound state problem in QCD, Chin. Phys. Lett. **37**, 121201 (2020).
[41] Z.-Q. Yao, D. Binosi, Z.-F. Cui, and C. D. Roberts, Semileptonic transitions: $B_{(s)} \to \pi(K)$; $D_s \to K$; $D \to \pi, K$; and $K \to \pi$, Phys. Lett. B **824**, 136793 (2022).
[42] R. Alkofer and L. von Smekal, The infrared behavior of QCD Green's functions. Confinement, dynamical symmetry breaking, and hadrons as relativistic bound states, Phys. Rep. **353**, 281 (2001).
[43] H. Sanchis-Alepuz, G. Eichmann, S. Villalba-Chávez, and R. Alkofer, Delta and Omega masses in a three-quark covariant Faddeev approach, Phys. Rev. D **84**, 096003 (2011).
[44] G. Eichmann and C. S. Fischer, Unified description of hadron-photon and hadron-meson scattering in the Dyson-Schwinger approach, Phys. Rev. D **85**, 034015 (2012).
[45] B. D. Keister and W. N. Polyzou, Relativistic Hamiltonian dynamics in nuclear and particle physics, Adv. Nucl. Phys. **20**, 225 (1991).
[46] J. Segovia, D. R. Entem, F. Fernandez, and E. Hernandez, Constituent quark model description of charmonium phenomenology, Int. J. Mod. Phys. E **22**, 1330026 (2013).
[47] S. J. Brodsky, E. Chudakov, P. Hoyer, and J. M. Laget, Photoproduction of charm near threshold, Phys. Lett. B **498**, 23 (2001).
[48] Y. Guo, X. Ji, and Y. Liu, QCD analysis of near-threshold photon-proton production of heavy quarkonium, Phys. Rev. D **103**, 096010 (2021).
[49] K. A. Mamo and I. Zahed, Diffractive photoproduction of J/ψ and Υ using holographic QCD: Gravitational form factors and GPD of gluons in the proton, Phys. Rev. D **101**, 086003 (2020).
[50] M. L. Goldberger and K. M. Watson, *Collision Theory* (Robert E. Krieger, Huntington, New York, 1975).
[51] H. Feshbach, *Theoretical Nuclear Physics: Nuclear Reactions* (John Wiley and Sons, New York, 1991).
[52] M. I. Haftel and F. Tabakin, Nuclear saturation and the smoothness off nucleon-nucleon potential, Nucl. Phys. A **158**, 1 (1970).
[53] A. Donnachie and P. V. Landshoff, Total cross sections, Phys. Lett. B **296**, 227 (1992).
[54] A. Donnachie and P. V. Landshoff, Exclusive vector meson production at HERA, Phys. Lett. B **348**, 213 (1995).
[55] A. Donnachie and P. V. Landshoff, Small x: two pomerons! Phys. Lett. B **437**, 408 (1998).
[56] T.-S. H. Lee, Pomeron-LQCD model of J/ψ photo-production on thenucleon, arXiv:2004.13934.
[57] J.-J. Wu and T.-S. H. Lee, Production of J/ψ on the nucleon and on deuteron targets, Phys. Rev. C **88**, 015205 (2013).
[58] Y. Oh and T.-S. H. Lee, One-loop corrections to ω photoproduction near threshold, Phys. Rev. C **66**, 045201 (2002).